View metadata, citation and similar papers at core.ac.uk
brought to you by CORE
provided by NASA Technical Reports Server

Retrieve Optically Thick Ice Cloud Microphysical Properties by Using Airborne Dual-Wavelength Radar Measurements

Zhien Wang
Department of Atmospheric Science
University of Wyoming
Dept. 3038 * 1000 E. University Avenue
Laramie, WY 82071

Gerald M. Heymsfield
NASA/Goddard Space Flight Center, Code 613.1, Greenbelt, MD 20771

Lihua Li
The GEST Center, University of Maryland Baltimore County
and
NASA/Goddard Space Flight Center, Code 613.1, Greenbelt, MD 20771

and

Andrew J. Heymsfield
NCAR, 3450 Mitchell Lane, Boulder, CO 80307

ABSTRACT

An algorithm to retrieve optically thick ice cloud microphysical property profiles is developed by using the GSFC 9.6 GHz ER-2 Doppler Radar (EDOP) and the 94 GHz Cloud Radar System (CRS) measurements aboard the high-altitude ER-2 aircraft. *In situ* size distribution and total water content data from the CRYSTAL-FACE field campaign are used for the algorithm development. To reduce uncertainty in calculated radar reflectivity factors (Z_e) at these wavelengths, coincident radar measurements and size distribution data are used to guide the selection of mass-length relationships and to deal with the density and non-spherical effects of ice crystals on the Z_e calculations. The algorithm is able to retrieve microphysical property profiles of optically thick ice clouds, such as, deep convective and anvil clouds, which are very challenging for single frequency radar and lidar. Examples of retrieved microphysical properties for a deep convective clouds are presented, which show that EDOP and CRS measurements provide rich information to study cloud structure and evolution. Good agreement between IWPs derived from an independent submillimeter-wave radiometer, CoSSIR, and dual-wavelength radar measurements indicates accuracy of the IWC retrieved from the two-frequency radar algorithm.

Keywords: dual-frequency or dual-wavelength radars, optically thick ice clouds, microphysical properties

1. INTRODUCTION

Ice clouds play a significant role in the atmospheric water and energy cycles [Wielicki et al. 1995]. High cold cirrus clouds affect the Earth's energy balance through both green-house and albedo effects. Because they are normally optically thin, we can observe cirrus with many different methods [Lynch et al. 2001]. There have been several research programs aimed at better understanding cirrus, most recently the Cirrus Regional Study of Tropical Anvils and Cirrus Layers-Florida Area Cirrus Experiment (CRYSTAL-FACE) field campaign (http://cloud1.arc.nasa.gov/crystalface/). However, the global net impact of cirrus is still unknown [Liou 1986; Lynch et al. 2001]. Deep convective and nimbostratus clouds are the main players in the atmospheric water cycle by redistributing water globally. The upper parts of these clouds are mainly ice and much of the condensate that does not reach the ground exits into the anvils of these clouds that can form extensive cirrus layers. These cirrus layers are important for the radiation budget. To improve our weather and climate forecast capability, accurate representations of ice regions are needed in models. This requires the advanced knowledge of the vertical distributions of ice cloud microphysical properties and their spatial and temporal variations in different types of ice clouds.

Although there are substantial advances in our remote sensing capability, it is still difficult to obtain microphysical property profiles in optically thick ice clouds, such as anvil clouds and upper parts of deep convective clouds. Algorithms based on lidar and radar measurements provide ice cloud microphysical property profiles [Donavan et al. 2001; Wang and Sassen 2002]. But these algorithms

can only be applied to ice clouds where the integrated optical depth reaches ~3 which lidar is able to penetrate. Algorithms using passive IR and solar radiance measurements can retrieve cloud properties with an optical depth larger than 3, but only for layer integrated properties. Algorithms using microwave measurements are best suited for optically thick cloud studies. Vertically integrated ice water pass (IWP) can be retrieved from space-based or airborne microwave and/or millimeter radiometer measurements [Vivekanandan et al. 1991; Weng and Grody 2000; Liu and Curry 2000; Evans et al. 2005]. To retrieve vertical ice water content (IWC) profiles of optically thick clouds, it is necessary to use cloud radar measurements. However, algorithms using single-frequency radar spectrum moments have difficulties when applied to convective clouds [Matrosov et al. 1994; Mace et al. 2003], and retrievals by using simple empirical IWC-radar reflectivity factor (Z_e) relationships usually have large uncertainties [Sassen et al. 2002].

Algorithms based on multi-frequency radar measurements are so far the best choice for profiling optically thick ice clouds. Atlas and Ludlam [1961] first explored information contained in multi-frequency radar measurements for hail determination. Recently, multi-frequency radar measurements were used for cirrus studies by Matrosov [1993] and Hogan et al. [1999, 2000] and for optically thick ice clouds by Sekelsky et al. [1999]. In general, these algorithms used information contained in the measurements due to the different contributions of Rayleigh and Mie scattering at different wavelengths. These studies indicated that the radar backscattering intensity of ice crystals in the Mie scattering region strongly depends on ice crystal shape, bulk density, size, and orientation. Due to lack of observations for justifying assumptions used in algorithm development, large uncertainties may be resulted in the retrievals and reducing these uncertainties is the major challenge of algorithm development based on multi-frequency radar measurements. The CRYSTAL-FACE field campaign 2002 provided a rich data set to allow us to examine the

necessary assumptions used for the algorithm development, so that we can use more realistic assumptions to improve the accuracy of the algorithm.

In this study, we will develop an algorithm to profile optically thick ice cloud microphysical properties by using airborne 9.6 and 94 GHz radar measurements from the NASA ER-2 high-altitude (~20 km) aircraft during the CRYSTAL-FACE field campaign. Compared with ground-based multi-frequency radar measurements, airborne measurements from the ER-2 avoid attenuation from moisture in the lower troposphere and precipitation often associated with deep ice clouds. These radars take advantage of higher radar sensitivity and higher resolution measurements of upper tropospheric clouds since the cloud top is closer to the radar. The observational data are briefly introduced in section 2. The algorithm development is presented in section 3. In section 4, a case study is presented to show the capabilities of the algorithm. Comparisons of IWC and IWP from different approaches are given in section 5 to further illustrate advantages of using multi-frequency radar measurements.

2. OBSERVATIONS

During July 2002, the CRYSTAL-FACE field campaign was conducted by NASA. Six aircraft equipped with a variety of remote sensors and *in situ* probes provided comprehensive measurements of aerosol, clouds, and atmospheric chemistry over the south Florida and surrounding region. The data used in this study are from two radars that flew on the NASA ER-2 aircraft, and *in situ* size distribution and total condensed water content (CWC) measurements from the University of North Dakota Citation aircraft.

The ER-2 Doppler radar (EDOP) is an X-band (9.6 GHz) Doppler radar mounted in the nose of a NASA ER-2. The instrument has two fixed antennas, one pointing at nadir and the second pointing approximately 33° ahead of nadir. This unique configuration enables EDOP to provide nadir measurements of reflectivity, vertical hydrometeor motion (and vertical air motion *w* after fallspeed removal), and along-track wind (*u*) and in the vertical plane mapped out by the ER-2. Additional details of the radar hardware and data processing are described by Heymsfield et al. [1996]. The cloud radar system (CRS) is a 94 GHz polarimetric Doppler radar developed for autonomous operation on a NASA ER-2 and for ground-based operation. On the ER-2, it is capable of detecting clouds and precipitation from the surface up to the aircraft altitude in the lower stratosphere. This radar is especially well suited for cirrus cloud studies because of its high sensitivity (-29 dBZ_e at 10 km range) and fine spatial resolution (e.g. 37.5 m in range). Its major data products include radar reflectivity, Doppler velocity, and velocity spectrum width. The details of the radar hardware and preliminary data are described by Li et al. [2004].

EDOP has been used in many field experiments dealing with convection and hurricanes as well as for Tropical Rain Measuring Mission (TRMM) validation. However, during CRYSTAL-FACE, it was the first time that EDOP and CRS flew together on the ER-2. This provided a unique opportunity to study optically thick ice clouds from a dual-wavelength perspective. EDOP and CRS data from the CRYSTAL-FACE and other field campaigns are available at http://meso-a.gsfc.nasa.gov/912/radar/.

The particle size distribution data used in this study were obtained from probes on the Citation aircraft that included the FSSP, 2D-C, 2D-P, HVPS and the Cloud Particle Imager (CPI). The size distributions are merged from the 2D-C and the HVPS data sets [Heymsfield et al. 2004] for a total

of 15814 5-second size distributions. Among these size distributions, only 49 were within 3 km spatially and 200 s temporally of the EDOP and CRS measurements. However, these coincident size distributions and radar measurements provide important constraints for the equivalent radar reflectivity factor (Z_e) calculations with the observed size distributions.

Lacking accurate size information for small ice crystals introduces additional uncertainties in IWC calculated from size distribution data. According to the recent study by Heymsfield et al. [2005] based on CRYSTAL-FACE *in situ* data, the small particles contribute about 10-20% of the total IWC depending on the total IWC. We will use this result to approximately account for the contribution of small ice crystals in IWC estimations from size distributions. Because the Z_e calculation is more sensitive to larger particles than the IWC calculation, we will neglect the contribution of small ice crystals in the Z_e calculation.

The CWC measured by the Counterflow Virtual Impactor (CVI) was also available from the Citation aircraft. Uncertainty for this CWC is estimated to be about 11% for a CWC of 0.2 g m^{-3}, but increases for smaller CWC [Twohy et al. 1997]. These measurements are important for constraining IWC calculated from measured size distributions. The *in situ* probes used here have sampling volumes ranging from 0.004 to 1 m^3s^{-1}. Therefore, the radar sampling volume is at least 3 orders higher than those of *in situ* probes. The miss-matched sampling volumes between the radar and the *in situ* measurements could be a serious issue for intercomparisons under situations of spatially inhomogeneous clouds.

In addition, the NASA Compact Scanning Submillimeter Imaging Radiometer (CoSSIR) flew on the ER-2 aircraft, and operated with 12 channels from a frequency of 183 to 640 GHz. The main

purpose of CoSSIR is for the retrieval of ice cloud properties [Wang et al. 2001]. The CoSSIR measurements can be used to estimate ice water path (IWP) [Evans et al. 2005]. The IWP retrieved from the CoSSIR will be used for comparison with the dual-wavelength algorithm discussed below.

3. ALGORITHM DEVELOPMENT

a. The forward Z_e calculation

The forward calculation of Z_e from the measured or assumed size distributions is an important step for developing multi-frequency radar measurement algorithms [Matrosov 1993; Hogan et al. 1999; Sekelsky et al. 1999] or single frequency radar algorithms [Austin and Stephens, 2001; Wang and Sassen 2002; Donovan et al. 2004]. Calculation of Z_e from a given ice crystal size distribution defined in terms of ice crystal maximum length first requires an ice crystal mass-length relationship to estimate the ice mass of a given size ice crystal. Then Z_e can be estimated based on the mass and size using appropriate scattering calculations. Different assumptions used in the forward calculations will result in uncertainties in developed algorithms. The CRYSTAL-FACE data are used here for providing more realistic assumptions in order to minimize the potential uncertainties caused by them.

In this study, we use measured size distributions rather than assuming a general size distribution. Therefore, the selection of a particle mass-length relationship is one of the major assumptions in the forward calculation. To determine the sensitivity to the mass-length relationship, we examine four mass-length relationships here. The first one is $m= 2.94\times10^{-3}\ D^{1.9}$ (B1995) for aggregates of unrimed bullets, columns, and side planes developed by Locatelli and Hobbs [1974] and recommended by Brown and Francis [1995]. Units of m and D are g and cm, respectively. The

second and third relations are derived from CRYSTAL-FACE data: $m = 5.13\times10^{-3}\ D^{2.1}$ (H2004), $m = 4.23\times10^{-3}\ D^{2.12}$ (E2004), by Heymsfield et al. [2004] and Evans et al. [2005], respectively. The ice crystal effective density can be defined as the total ice crystal mass divided by the volume of a sphere with the diameter of maximum ice crystal length. Therefore, a mass-length relationship gives the effective density of ice crystals as a function of crystal size. According to Heymsfield et al. [2004], typical values for effective density range from near 0.91 g cm^{-3} for sub-100-μm pristine ice crystals to near 0.01 g cm^{-3} for large aggregates. However, these power-law relationships give very small effective density values for large ice crystals and effective density values larger than solid ice for small ice crystals. To avoid these limitations of a simple power-law particle mass-length relationship, it is necessary to set the upper and lower limits of effective density values defined by a power-law relationship or to use more complicated mass-length relationship formulation. Therefore, we assume a modified mass-length relationship of $m = 1.25\times10^{-3}\ D^{1.7}$ (TEST) that sets the upper and lower limits of effective densities to 0.89 and 0.02 g/cm^3, respectively. These density bounds are based on the coincident *in situ* size distributions and radar measurements as discussed below. The ice crystal effective densities defined by these four relationships are presented in the Fig. 1, and the differences among small and large size ice crystals are obvious.

The particle mass-length relationships were developed originally for ice water content (IWC) estimations based on the measurements from ice particles sampled at the ground [Locatelli and Hobbs, 1974]. Therefore, a mass-length relationship, which gives reasonable estimates of IWC, does not guarantee an accurate Z_e estimation because Z_e is more sensitive to larger particles than IWC [Heymsfield et al. 2005; Wang et al. 2004]. Figure 2 shows the scatter-plot of the IWC ratio

between CVI measured and calculated using the four particle mass-length relationships given in Fig. 1. To determine the contribution of small particles in the IWC calculation, we simply increase the calculated IWC by 15% according to the recent study of Heymsfield et al. [2005]. Though the values of IWC ratio have considerable scatter, these four relationships provide similar calculated IWC. However, there can be a few dB differences in Z_e values when using different particle mass-length relationships, while IWC calculations do not vary significantly with the size distribution [Wang et al. 2004; Heymsfield et al. 2005]. This point will be further illustrated below.

When particle size is large compared with radar wavelength, we need to consider Mie scatter effects in the Z_e calculations. Studies have shown that the scattering by large ice crystals at radar wavelengths depends strongly on ice crystal size, shape and orientation [Matrosov 1993; Liu and Illingworth 1997; Hogan and Illingworth 1999; Sekelsky et al. 1999; Hogan et al. 2000; Okamoto 2002; Donovan et al. 2004]. For particles with the same mass and shape, the bulk densities of ice particles also affect the Z_e calculation. Therefore, it is not an easy task to estimate the radar backscattering of irregular ice particles. This has become a major challenge for developing multi-frequency radar algorithms for ice clouds and precipitation-sized solid ice. The results of T-Matrix calculations [Mishchenko and Travis 1998] presented in Fig. 3 simply illustrate the sensitivity of radar backscattering to these factors.

The backscattering intensities of sphere and prolate spheroids with different bulk densities at 9.6 and 94 GHz are represented in Fig. 3 as a function of the radius of the solid ice mass equivalent sphere (R_{solid}). The prolate spheroids may be not able to accurately represent complex ice crystal shapes, but we use them here only to show radar backscattering sensitivity to ice crystal shapes. As indicated in Fig. 3a, the effects of Mie scatter and shapes at 9.6 GHz are small when R_{solid} of the ice crystal is smaller than ~1.5 *mm*. Particles with this R_{solid} value are very large ice crystals in terms of

ice crystal maximum length. However, noticeable differences in the 94 GHz Z_e when R_{solid} is larger than ~0.2 *mm* are caused by different ice crystal shapes and bulk densities. These results are consistent with calculations using different shapes and scattering calculation techniques [Liu and Illingworth 1997; Okamoto 2002; Donovan et al. 2004]. In deep and/or optically thick ice clouds, most of ice crystals have sizes beyond 0.2 *mm*. Considering the large variations of ice crystal shape and density in different types of clouds, providing an effective approximation for calculating Z_e for ice crystals in the Mie scattering region is difficult, but required here. The CRYSTAL-FACE data provide an opportunity to refine the Z_e calculation and to develop a more accurate approach.

To retrieve ice crystal generalized effective size (D_{ge}, defined by Fu 1996) and IWC from multi-frequency radar measurements, we need to rely on ice crystal backscattering intensity differences at different radar frequencies caused by Rayleigh and Mie scattering. Therefore, we have to treat Mie scattering properly in order to have accurate retrievals. As illustrated in Fig. 3, the 9.6 GHz Z_e calculation is only slightly affected by Mie scatter, and we need to consider Mie scattering at 94 GHz when particle length is larger than a few hundred micrometers. Therefore, the forward Z_e calculation at 9.6 GHz is much simpler than that at 94 GHz.

As discussed above, the selection of a mass-length relationship is a main factor affecting 9.6 GHz Z_e calculations. The impacts of different mass-length relationships on the 9.6 GHz Z_e calculation are shown in Fig. 4 based on coincident *in situ* particle size distributions and radar measurements. There is a large variation of the ratio between calculated Z_e and EDOP-measured Z_e for each relationship. This highlights the difficulties of inter-comparing ice cloud *in situ* measurements with radar measurements since sample volumes are totally different and the measurements may differ from ice cloud spatial inhomogeneity. However, there are noticeable differences among different particle mass-length relationships. It is clear that the mean Z_e ratios of B1995, E2004, and H2004

increase with the increase of observed Z_e. This bias is partly corrected in the TEST relationship. For the observed Z_e below -10 dBZ, the calculated Z_e values of H2004 and TEST are similar. However, the calculated Z_e values differ by a factor of 2 for Z_e above -10 dBZ, and this is mainly caused by distributing ice mass differently among different size particles. Based on this comparison, we conclude that the TEST relationship gives a better 9.6 GHz Z_e calculation.

As indicated in Fig. 3, it is more complicated to calculate 94 GHz Z_e because the assumptions of ice crystal shape, bulk density, and mass-length relationships have significant impacts on it. Given a mass-length relationship, we know the mass of an ice particle from its size. In the Mie scattering regime, we also need to know the ice particle shape and its size or bulk density in order to calculate accurate 94 GHz Z_e. Although the backscatter of some ice crystal shapes have been calculated accurately at radar wavelengths [Matrosov, 1993; Aydin and Tang, 1997; Okamoto, 2002], it is difficult to choose an ice crystal shape or an ensemble of shapes that represent the general non-spherical effects of the variety of ice crystal shapes in ice clouds. Donovan et al. [2004] indicated that the equivalent area or equivalent mass solid ice sphere representation for irregular particles performs well compared with the discrete-dipole approximation (DDA) calculation for ice crystal size below 1000 μm. In general, we still do not have sufficient knowledge to accurately account for both the shape and density effects of large ice crystals on the 94 GHz Z_e calculation. Here, we search for a simple but effective approach to reasonably take both effects into account by using CRYSTAL-FACE data.

Similar to the 9.6 GHz Z_e calculation, we use coincident *in situ* and radar observations to guide the 94 GHz Z_e calculation [Wang et al. 2004]. However, co-incident data are very limited and mainly occurs when 9.6 GHz Z_e values are below 10 dBZ. One way to overcome these limitations is to compare statistical relationships obtained from the radar data with *in situ* size distributions with the

assumption that both sources of information provide a typical sampling of the cloud system. Figure 5 presents a frequency distribution of dual-wavelength-ratio (DWR) between 9.6 and 94 GHz as a function of 9.6 GHz Z_e based on CRYSTAL-FACE observations. For a given 9.6 GHz Z_e, there is a wide distribution of DWR. This clearly indicates that the ice crystal size distributions are varying widely in nature; therefore, it is difficult to estimate IWC from a single-frequency radar Z_e measurement.

A simple approximation for irregular ice crystals is to use different equivalent spheres to represent the crystal, and then use Mie scattering to calculate the particle scattering properties [Donovan et al. 2004]. The first approach tested here is to convert the total ice crystal mass estimated from the mass-length relationship into a solid sphere. The second approximation is to assume a sphere represented by an ice-air mixture with a calculated equivalent diameter from the maximum particle length and total ice mass. Calculated DWRs as a function of calculated 9.6 GHz Z_e for these two approaches are given in Figs. 6a and 6b. The solid line is the observed mean DWR-Z_e relationship discussed in Fig. 5. It is clear that the first approach produces much smaller DWR than the observed and the second approach produces a larger DWR than the observed when 9.6 GHz Z_e is above 20 dB. Smaller-sized solid equivalent spheres used in the first approach introduce a weak Mie scatter effect and therefore over-estimate 94 GHz Z_e. On the other hand, larger size spheres used in the second approach introduce a strong Mie scattering effect and underestimate 94 GHz Z_e.

The goal here is to develop an approach that provides a DWR and 9.6 GHz Z_e that approximates the CRS and EDOP observations. Figures 6a and 6b suggest that an approach assuming a spherical ice particle with size and bulk density between first and second approaches may be appropriate. This idea is tested by modifying the second approach by fixing the bulk density of particles with a maximum length larger than 2800 μm to be 0.2 g cm^{-3}. This modification approximates the large

particles with smaller size and higher bulk density equivalent spheres than those used in the second approach. According to the calculations given in Fig. 3, this modification for large particles can reduce the Mie scattering effects in the Z_e calculations. The calculated DWR and 9.6 GHz Ze with this approach are given in Fig. 6c, which shows a better agreement with the observed mean relationship. The calculations with this approach are also over plotted in Fig. 5 (scatter black dots) and have good agreement with the observed DWR frequency distributions.

DWR is the main parameter used to retrieve cloud microphysical properties from dual-wavelength radar measurements. The above discussion indicates that the third approach can provide a reasonably good DWR calculation, at least from a statistical point of view. Therefore, we use this approach for the 94 GHz Z_e calculation. To further evaluate this approach, Fig. 7 shows the IWC ratio, the ratio of the calculated IWC and the CVI measured IWC, as functions of the 9.6 GHz Z_e and the DWR. Each point corresponds to a 5-s average *in situ* size distribution. To illustrate trends better, the averaged IWC ratio for a given Z_e or the DWR bin is plotted with triangle symbols, and the solid line represents an IWC ratio of one. Although the individual ratios have considerable scatter, the mean ratio is very close to one over a wide range of Z_e and DWR. These results not only show that our IWC calculations based on size distributions have good accuracy, but it also illustrates that the approaches used here for Z_e calculations are reliable. The comparison of calculated Z_e and observed Z_e for coincident observations is given in Fig. 8. The calculated and observed Z_e are scattered around the 1:1 line with most of points within ± 3dB of this line. This suggests the validity of the above approach that uses statistical properties from the measurements.

b. The retrieval of ice cloud microphysical properties

With above discussion, we are able to develop relationships among IWC, D_{ge}, Z_e and DWR with confidence. The mean ratio of 9.6 GHz Z_e to IWC as function of DWR is presented in Fig. 9a. The standard deviation values are within ~30% of the mean value, and this reflects the natural variations of cloud properties and uncertainties resulting from the assumptions. Here, we use the mean relationship to retrieve IWC from 9.6 GHz Z_e and DWR. As shown in Fig. 8, there are almost no IWC biases in terms of DWR and 9.6 GHz Z_e. Therefore, we simply use these standard deviations to estimate the retrieval uncertainty of IWC. The approach used here is simple compared to more systematic treatments of retrieval errors [Austin and Stephens, 2001; Mace et al. 2002; Evans et al. 2005]. However, the standard deviation statistics should provide reasonable estimates of statistical uncertainties, and they are readily applied to the observations.

There is a ~1.27 dB difference between 9.6 GHz and 94 GHz Z_e in Rayleigh scattering regions due to the different water dielectric constants. Therefore, 1.27 is added to DWR for fitting the ratio of 9.6 GHz Z_e to IWC as function of DWR. The fitted relationship is $y = a + bx + cx^2$, where $x = log(DWR+12.7)$, $y = ln(10^{0.723}Z_e/IWC)$, and a, b, and c are constants. The values for a, b, and c are 2.59324, 3.17094, and 0.137975; 3.00510, 0.337015, and -0.00263462 for $DWR+12.7 \leq$ and $>$ 7.94328 dB, respectively. The relative uncertainty of observed DWR increases when DWR is below -0.5 dB; this will also increase the retrieved IWC uncertainty. Small DWR regions are usually located in the upper regions of clouds where particle sizes are relatively small and can be detected by the Cloud Physics Lidar (CPL) on the ER-2. Combining CPL and CRS measurements covers the overlap regions that may not be detected by the 9.6 GHz EDOP radar [Wang and Sassen 2002]. In the current retrieval, we do not apply the dual-wavelength approach when DWR is below -0.5 dB, and instead we use a Z_e-IWC relationship to obtain IWC in this situation.

Similarly, we can develop a relationship between D_{ge} and DWR. We use the general definition of D_{ge} given by Fu [1996]:

$$D_{ge} = \frac{2}{\sqrt{2}\rho_i}\frac{IWC}{A_c}, \qquad (1)$$

where A_c is the cross-sectional area of ice crystals per unit volume and ρ_i is solid ice density. By using the cross-sectional area of ice cloud particles parameterized by Heymsfield and Miloshevich [2003], we can calculate A_c from the measured size distributions and then combine this IWC to derive D_{ge}. According to Heymsfield and Miloshevich [2003], the A_c of ice crystal depends on ice crystal shape as well as ice crystal length. Like the IWC calculations from *in situ* size distributions, the uncertainty for the D_{ge} calculation for a given size distribution is also large. However, the mean properties of D_{ge} from a large data set should have a better accuracy from a statistical point of view. The mean D_{ge} as a function of DWR is presented in Fig. 9b and it is used to develop relationship between D_{ge} and DWR for the retrieval. Similar to the IWC retrieval, we use the standard deviation of mean D_{ge} to characterize the D_{ge} retrieval uncertainty.

For optically thick ice clouds, we also need to consider the attenuation by cloud particles at 94 GHz. Because of the strong Mie scattering effect at 94 GHz, it is challenging to correct for attenuation properly when only 94 GHz measurements are available. For dual-wavelength measurements, we can estimate the 94GHz attenuation by using the retrieved IWC and D_{ge}. The main goal of correcting for 94 GHz attenuation is to have a better DWR estimate to improve the retrieval accuracy of IWC, especially for convective clouds. Therefore, an iterative step is required for correcting the 94 GHz attenuation using IWC and D_{ge}. A simple approach is to use the 9.6 GHz Z_e as an indicator of 94 GHz attenuation. Figure 10 shows one way 94 GHz attenuation coefficients as a function of 9.6 GHz Z_e based on CRYSTAL-FACE *in situ* size distributions. When 9.6 GHz Z_e is

below 15 dBZ, there is a large range of attenuation coefficients at 94 GHz. Fortunately, the attenuation coefficient is relatively small for this Z_e range, therefore, we can use mean attenuation coefficients without large uncertainties in the attenuation correction. The curve fitted to the mean values shown in Fig. 10 is used for the 94 GHz attenuation corrections.

4. CASE STUDY

To demonstrate the retrieval algorithm capability and its potential applications, we present cross-sections from three flight lines across a convective system observed on 29 July 2002 during CRYSTAL-FACE. Figure 11 displays a sequence of GOES 8 IR channel (10.8 μm) images observed on 29 July 2002 during these flight lines. In each GOES image, the flight track closest to the image time (solid black lines) and its time period are indicated. The GOES images clearly indicate the development of the cloud systems during the ER-2 flight. The two sea-breeze initiated convective regions initially developed from the east and west shores of the southern Florida around 1700 UTC, then the anvils from each convective system merged after 1930 UTC as the systems matured. After 2030 UTC, we can not separate the two convective cells in the GOES IR image. The ER-2 measurements were mainly focused on the westernmost convective region as indicated by the flight tracks.

The CRS and EDOP Z_e measurements from the ER-2 (Figs. 12a, 12b) provide unique vertical cross sections through the convective region for three selected time periods (1942-1959, 2023-2040, and 2043-2101 UTC). These sections cut through a decaying region of the convection that appears as a deep ice region aloft with light rain near the surface. Comparison of the 94 and 9.6 GHz measurements clearly indicates strong Mie scattering in the 94 GHz measurements since the 94

GHz Z_e is significantly less than the 9.6 GHz Z_e in the lower part of the ice cloud region. The bright-band at approximately the freezing level altitude is evident in the 9.6 GHz observations, and the dual-wavelength approach discussed above can be used for the retrieval of ice cloud microphysical properties above the bright-band. However, this approach would not be useful for the initial developing stage of convective clouds because of the potential existence of mixed-phase clouds above freezing level.

The retrieved IWC and D_{ge} images presented in Figs. 12c and 12d show interesting evolution of the microphysical structure. Though this may be partially caused by the position of the flight track relative to the storm center, the differences appear to be mostly related to the storm-scale dynamics and cloud physics processes. The larger convectively-generated particles fall out first since they have higher fallspeeds; therefore large particles are mainly located near the cloud base as revealed by D_{ge} images (Fig. 12 d-1 to d-3). Interestingly, the higher IWC regions usually correspond to regions with smaller particles. The data suggests that large ice particles were initially released aloft by a convective anvil, and then these particles sedimented out of the cloud. There is a noticeable decrease in the height and size of the high IWC region between the first and third flight line, a period of about 1-hour. By the third flight line, the drizzle below the cloud layer strengthens as the larger particles sediment out. In future research, combining these retrievals with other observations and model simulations are needed to further understand the storm structure and its evolution.

5. IWC and IWP Comparison with the other approaches

The case study in last section illustrates the excellent microphysical profiling capability by combining CRS and EDOP measurements. The IWC comparison given in Fig. 13 further illustrates the advantage of using dual-wavelength radar measurements (Fig. 13a) compared with single

frequency radar measurements (Figs. 13 b-f). For single frequency radar measurements, we can use IWC-Z_e relationships to estimate the IWC profile [Sassen, 1987; Liu and Illingworth, 2000]. However, the uncertainties in IWC from these relationships can be large when they are applied to situations significantly different from the datasets they were derived from [Sassen et al., 2002]. Here three single-frequency 94 GHz IWC-Z_e relationships are used for comparison: IWC=0.137 $Z_e^{0.643}$ (L2000, Fig. 13b) proposed by Liu and Illingworth [2000], IWC=0.11 $Z_e^{0.63}$ (M2001, Fig. 13c) proposed by Matrosov [Sassen et al. 2002], and Z_e= 4.0 $IWC^{1.58}$ (IWC <0.059 g m^{-3}) and Z_e= 54.8 $IWC^{2.5}$ (IWC >0.059 g m^{-3}, Fig. 13d) proposed by Heymsfield et al. [2005]. According to Sassen et al. [2002], the first two relationships perform well for cirrus clouds. Two relationships for 9.6 GHz are used: 1) IWC=0.097 $Z_e^{0.5}$ (Fig. 13e), and 2) Z_e= 8.9 $IWC^{1.66}$ (IWC <0.059 g m^{-3}) and Z_e= 178.6 $IWC^{2.72}$ (IWC >0.059 g m^{-3}, Fig. 13f) proposed by Heymsfield et al. [2005]. In general, the IWC-Z_e relationships for the same radar frequency give similar IWC structure, and there are big differences between 9.6 and 94 GHz relationships. Compared with the retrievals by the dual-wavelength radar approach (Fig. 13a), the IWC-Z_e relationships for 94 GHz underestimate high IWC and the IWC-Z_e relationships for 9.6 GHz overestimate IWC. For this case, the 94 GHz measurements provide a more realistic vertical IWC structure. The difference between 9.6 and 94 GHz is mainly caused by the strong Mie scattering effects observed at 94 GHz.

One way to evaluate the performance of the dual-wavelength algorithm is to compare vertically integrated ice water path (IWP) obtained by CoSSIR. Figure 14 presents an intercomparison of IWPs retrieved from the CoSSIR nadir measurements [Evans et al. 2005], the dual-wavelength radar measurements, and those estimated using IWC-Z_e relationships. Although CoSSIR measurements are unable to provide an accurate IWC profile, they can be used to retrieve reliable

IWP [Evans et al. 2005]. Three columns in Fig. 14 represent three different days, and from left to right are for July 29, 28, and 3, respectively. The time series of IWP from CoSSIR and dual-wavelength retrievals are compared in row "a". There is good agreement between them when IWP values are larger than 100 g m^{-2}. The scatter plots comparing CoSSIR IWP with IWPs from dual-wavelength approach, and two Z_e-IWC relationships are given in rows "b" to "d". The limitation of current CoSSIR measurements for retrieval of small IWP is clear in the scatter plots. Figure 14b indicates a good correlation between CoSSIR IWP and dual-wavelength derived IWP from 100 up to 20000 g m^{-2}. However, IWPs derived from the IWC-Z_e relationships (L2000 and M2001) only have a good correlation with CoSSIR IWP from 100 up to 1000 g m^{-2}, then begin to underestimate IWP above 1000 g m^{-2}. The consistency between the IWP derived from CoSSIR measurements and from the dual-wavelength radar measurements suggests some validity to the dual-wavelength approach developed here. This intercomparison also clearly indicates the advantage of dual-wavelength radar approach over simple IWC-Z_e relationships.

6. SUMMARY

An algorithm using the EDOP and CRS measurements from the ER-2 aircraft is developed to retrieve optically thick ice cloud microphysical property profiles. For algorithm development, we need to accurately calculate the 9.6 and 94 GHz Z_e from the observed *in situ* size distributions. According to scattering calculations, 94 GHz Z_e is more sensitive to ice crystal shapes, size, and bulk density than 9.6 GHz Z_e. The coincident *in situ* size distribution data and radar measurements obtained during the CRYSTAL-FACE field campaign provide a unique chance to refine the calculations of 9.6 and 94 GHz Z_e. With the guidance of observations, we selected a particle mass

length relationship to provide a better 9.6 GHz Z_e calculation, and developed a simple approach to account for Mie scatter and non-spherical effects in the 94 GHz Z_e calculation.

The results clearly indicated that assumptions and approximations used in the algorithm development provide unbiased IWC estimation in larger ranges of DWR and 9.6 GHz Z_e by comparing with CVI measured IWC. The observational constraints give us a higher confidence in the developing relationships for IWC and D_{ge} retrievals. Mean relationships between IWC and D_{ge} with DWR and 9.6 GHz Z_e are developed and used for IWC and D_{ge} retrievals. The standard deviations of mean values are used to estimate retrieval uncertainties. To improve DWR estimation from 94 and 9.6 GHz Z_e measurements, ice cloud attenuation at 94 GHz is approximately corrected by using unattenuated 9.6 GHz measurements.

The capability of the approach is illustrated with a decaying convective region observed during CRYSTAL-FACE. With the airborne dual-wavelength radar measurement, we are able to provide high spatial resolution cloud microphysical properties, which are not possible from *in situ* sampling at a single altitude and from single frequency radar measurements. The good agreement IWP derived from the dual-wavelength approach and from CoSSIR measurements indicates reasonable accuracy of our IWC retrievals. The case study also shows that this kind of airborne profiling capability provides important information to study the evolution of convective clouds and other optically thick ice clouds. The high resolution data also provide a more effective way to compare the radar observations with cloud resolving model simulations. In the future, we will combine cloud retrievals with other observations and model simulations to better understand cloud physics and dynamics. The retrieved results have many other applications, for example, providing a database for passive remote sensing algorithm development and for improving the CloudSat retrieval for optically thick clouds.

ACKNOWLEDGMENTS

This work was supported by the NASA Radiation Sciences Program under the CRYSTAL-FACE funding 622-45-06. We are appreciative of the help from Dr. Lin Tian of GEST and Mr. Larry Belcher of SSAI on the radar data processing and other issues related to the data.

REFERENCES

Atlas, D., and F. H. Ludlam (1961), Multi-wavelength radar reflectivity of hailstorms, *Quart. J. Roy Meteor. Soc.*, *87*, 523-534.

Austin, R. T., and G. L. Stephens (2001), Retrieval of stratus cloud microphysical parameters using millimetric radar and visible optical depth in preparation for CloudSat, Part I: Algorithm formulation, *J. Geophys. Res.*, *106*, 28,233- 28,242.

Brown, P. R., A., and P. N. Francis (1995), Improved measurements of the ice water content in cirrus using a total-water probe, *J. Atmos. Oceanic Tech.*, *12*, 410-414.

Donovan, D. P., M. Quante, I. Schlimme, and A. Macke, (2004), Use of equivalent spheres to model the relation between radar reflectivity and optical extinction of ice cloud particles. *Appl. Opt.*, *43*, 4929-4940.

Donovan, D. P. and A. C. A. P. Van Lammeren (2001), Cloud effective particle size and water content profile retrievals using combined lidar and radar observations, 1, theory and examples. *J. Geophys. Res.*, *106*, 27425-27448.

Evans, K. F., J. R. Wang, P. E. Racette, G. M. Heymsfield, and L. Li (2005), Ice cloud retrievals and analysis with the compact scanning submillimeter imaging radiometer and the cloud radar system during CRYSTAL-FACE, *J. Appl. Meteor.*, in press.

Fu, Q. (1996), An accurate parameterization of the solar radiative properties of cirrus clouds for climate models, *J. Climate*, *9*, 2058-2082.

Heymsfield, A. J., and L. M. Miloshevich (2003), Parameterizations for the cross-sectional area and extinction of cirrus and stratiform ice cloud particles, *J. Atmos. Sci.*, *60*, 936-956.

Heymsfield, G. M., S. W. Bidwell, I. J. Caylor, A. S., S. Nicholson, W. C. Boncyk, L. Miller, D. Vandemark, P. E. Racette, and L. R. Dod (1996), The EDOP radar system on the high-altitude NASA ER-2 aircraft, *J. Atmos. Ocean. Tech.*, *13*, 795–809.

Heymsfield, A. J., A. Bansemer, C. Schmitt, C. Twohy, M. R. Poellot (2004), Effective ice particle densities derived from Aircraft data, *J. Atmos. Sci.*, *61*, 982-1003.

Heymsfield, A. J, Z. Wang, and S. Matrosov (2005), Improved radar ice water content retrieval algorithms using coincident microphysical and radar measurements, *J. Appl. Meteor.*, in press.

Hogan, R. J., and A. J. Illingworth (1999), The potential of spaceborne dual-wavelength radar to make global measurements of cirrus clouds, *J. Atmos. Oceanic Tech.*, *16*, 518-531.

Hogan, R. J., A. J. Illingworth, and H. Sauvageot (2000), Measuring crystal size in cirrus using 35 and 94 GHz Radars, *J. Atmos. Oceanic Tech.*, *17*, 27-37.

Li, L., G. M. Heymsfield, P. E. Racette, T. Lin, and E. Zenker (2004), A 94 GHz cloud radar system on a NASA high-altitude ER-2 aircraft, *J. Atmos. Oceanic Tech.*, *21*, 1378-1388.

Liou, K. N. (1986), Influence of cirrus clouds on weather and climate processes: A global perspective, *Mon. Wea. Rev.*, *114*, 1167-1199.

Liu, Chun-Lei, and A. J. Illingworth (1997), Error analysis of backscatter from discrete dipole approximation for different particle shapes, *Atmos. Res.*, *44*, 231-241.

Liu, C., and A. J. Illingworth (2000), Toward more accurate retrievals of ice water content from radar measurements of clouds, *J. Appl. Meteor.*, *39*, 1130-1146.

Liu, G. and J. A. Curry (2000), Determination of ice water path and mass median particle size using multichannel microwave measurements, *J. Appl. Meteor.*, *39*, 1318-1329.

Locatelli, J. D., and P. V. Hobbs (1974), Fall speeds and masses of solid precipitation particles, *J. Geophys. Res.*, *79*, 2185-2197.

Lynch, D. K., K. Sassen, A. Del Genio, A. Heymsfield, P. Minnis, M. Platt, M. Quante, U. Schumann, and H. Sundqvist (2002), Cirrus: The future, in *Cirrus*, edited by D. Lynch, K. Sassen, D. O C. Starr and G. Stephens, Oxford University Press.

Mace, G. G., A. J. Heymsfield, and M. R. Poellot (2002), On retrieving the microphysical properties of cirrus clouds using the moments of the millimeter-wavelength Doppler spectrum, *J. Geophys. Res.*, *107*, DOI 10.1029/2001JD001308.

Matrosov, S. Y. (1993), Possibilities of cirrus particles sizing form dual-frequency radar measurements, *J. Geophys. Res.*, *98*, 20,675-20,683.

Matrosov, S. Y.,B. W. Orr, R. A. Kropfli, J. B. Snider (1994), Retrieval of vertical profiles of cirrus cloud microphysical parameters from Doppler radar and infrared radiometer measurements, *J. Appl. Meteor.*, *33*, 617-626.

Mishchenko, M. I., and L. D. Travis (1998), Capabilities and limitations of a current Fortran implementation of the t-matrix method for randomly oriented, rotationally symmetric scatters, *J. Quant. Spectrosc. Radiat. Transfer*, *60*, 309-324.

Okamoto, H. (2002), Information content of the 95-GHz cloud radar signals: Theoretical assessment of effects of nonsphericity and error evaluation of the discrete dipole approximation, *J. Geophys. Res.*, ***107***, 4628, doi:10.1029/2001JD001386.

Sassen, K., Z. Wang, V. I. Khvorostyanov, G. L. Stephens and A. Bennedetti (2002), Cirrus cloud ice water content radar algorithm evaluation using an explicit cloud microphysical model, *J. Appl. Meteor.*, *41*, 620-628.

Sekelsky, S. M., W. L. Ecklund, J. M. Firda, K. S. Gage, and R. E. McIntosh (1999), Particle size estimation in ice-phase cloud using multifrequency radar reflectivity measurements at 95, 33, and 2.8 GHz, *J. Appl. Meteor.*, *38*, 5-28.

Twohy, C. H., A. J. Schanot, and W. A. Cooper (1997), Measurement of condensated water content in liquid and ice clouds using an airborne counterflow virtual impactor, *J. Atmos. Oceanic Tech.*, *14*, 197-202.

Vivekanandan, J., J. Turk, and, V. N. Bringi, (1991), Ice water path estimation and characterization using passive microwave radiometry, *J. Appl. Meteor.*, *30*, 1407-1421.

Wielicki, B. A., R. D. Cess, M. D. King, D. A. Randall, and E. F. Harrison (1995), Mission to planet earth: role of clouds and radiation in climate, *Bull. Amer. Meteor. Soc.*, *76*, 2125-2153.

Wang, J. R., G. Liu, J. D. Spinhirne, P. Racette, and W. D. Hart (2001), Observations and retrievals of cirrus cloud parameters using multichannel millimeter-wave radiometric measurements, *J. Geophys. Res.*, *106*, 15,251-15,236.

Wang, Z. and K. Sassen (2002), Cirrus cloud microphysical property retrieval using lidar and radar measurements: I algorithm description and comparison with *in situ* data, *J. Appl. Meteor.*, *41*, 218-229.

Wang, Z., G. M. Heymsfield, L. Li, and A. J. Heymsfield (2004), Ice cloud microphysical property retrieval using airborne two-frequency radars, in *Microwave Remote Sensing of the Atmosphere and Environment IV, Proceeding of SPIE, 5654*, edited by G. S. Jackson and S. Uratsuka, pp. 48-56, SPIE.

Weng, F., and N. C. Grody (2000), Retrieval of ice cloud parameters using a microwave imaging radiometer, *J. Atmos., Sci., 57*, 1069-1083.

Figure Captions

Figure 1. Ice crystal effective density as a function of ice crystal maximum length defined by different mass-length relationships. See text for more details.

Figure 2. The ratio of calculated IWC with CVI measured as a function of CVI measured IWC. Each panel corresponds to a mass-length relationship given in Fig.1. Note the contribution of missed small ice crystals is assumed to be ~15% of the total IWC on average.

Figure 3. The 9.6 and 94 GHz backscattering intensities of different shape and bulk density ice crystals as a function of the radius of the solid mass equivalent ice sphere. Spheres and prolate spheroids with different aspect ratios are indicated by different line styles, and different bulk densities are shown with different gray shades.

Figure 4. The ratios of calculated and observed 9.6 GHz Z_e as a function of observed 9.6 GHz Z_e for four different mass-length relationships based on coincident observations

Figure 5. The DWR-Z_e relationship based on CRS and EDOP observations during the CRYSTAL-FACE. The solid line is the mean DWR whereas the black dots are calculated results based on the *in situ* size distributions.

Figure 6. Calculated DWR-Z_e relationships from three different approaches. The solid line represents the mean relationship observed from CRYSTAL-FACE.

Figure 7. The IWC ratio of calculated and CVI measured as functions of 9.6 GHz Z_e and DWR between 9.6 and 94 GHz. The solid lines indicate the ratio of one, and triangle symbols represent mean ratios within given bin sizes.

Figure 8. Comparison of calculated Z_e with observed Ze at 9.6 and 94 GHz for collocated radar and *in situ* observations. The solid line is the 1:1 line and the dashed lines indicate a ± 3dB region about the 1:1 line.

Figure 9. The mean and standard deviation of IWC and D_{ge} as a function of DWR between 9.6 and 94 GHz calculated based on all *in situ* size distribution data from the CRYSTAL-FACE. The vertical bars indicate the standard deviation about the mean.

Figure 10. The 94 GHz attenuation coefficient of ice clouds as a function of Z_e at 9.6 GHz. The solid line is a fitted result, and diamond symbols represent means at given Z_e bins. The mean attenuation coefficients for different Z_e bins are represented by diamonds. The solid line is the fitted result of mean values.

Figure 11. GOES IR images with ER-2 flight tracks (solid black lines) during six periods observed on 29 July 2002 over the west coast of Florida. The solid lines over cloud decks are ER-2 flight tracks with arrows indicating the flight direction.

Figure 12. The time-height cross-sections of observed 9.6 and 94 GHz Z_e and retrieved IWC and D_{ge} for three flight tracks given in Fig. 11. Each column represents a flight track with time period given at the top. Note the color scales are different for 94 and 9.6 GHz Z_e. The cross-sections are plotted in the same east-to-west orientation with west on the left side.

Figure 13. IWC comparison from different approaches: a) dual-wavelength radar approach discussed in this paper, 94 GHz Z-IWC relationships of (b) Liu and Illingworth (2000), (c) Matrosov (2002), and (d) Heymsfield et al. (2005), and 9.6 GHz Z-IWC relationships of (e) $IWC=0.097*Z_e^{0.5}$ and (f) Heymsfield et al. (2005).

Figure 14. The intercomparison of IWP derived from the dual-wavelength radar approach, CoSSIR, and two Z-IWC relationships based on measurements on 3, 28 and 29 July 2002 during the CRYSTAL-FACE.

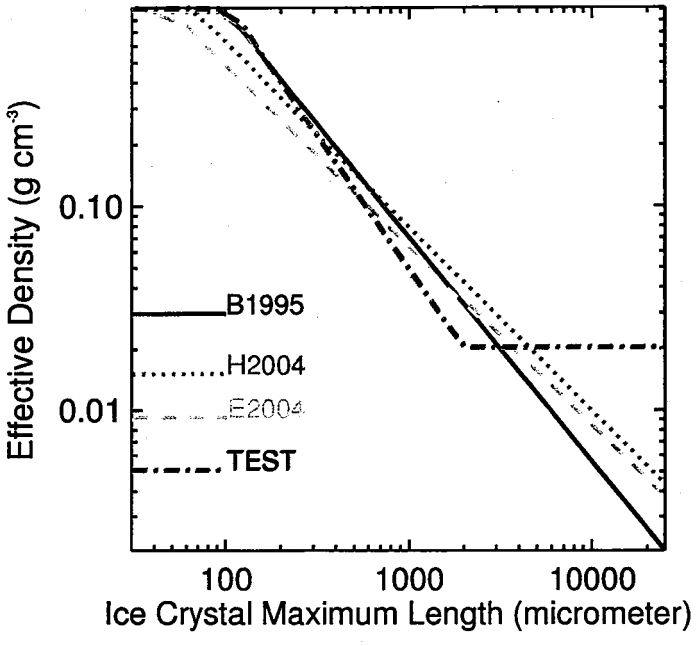

Figure 1. Ice crystal effective density as a function of ice crystal maximum length defined by different mass-length relationships. See text for more details.

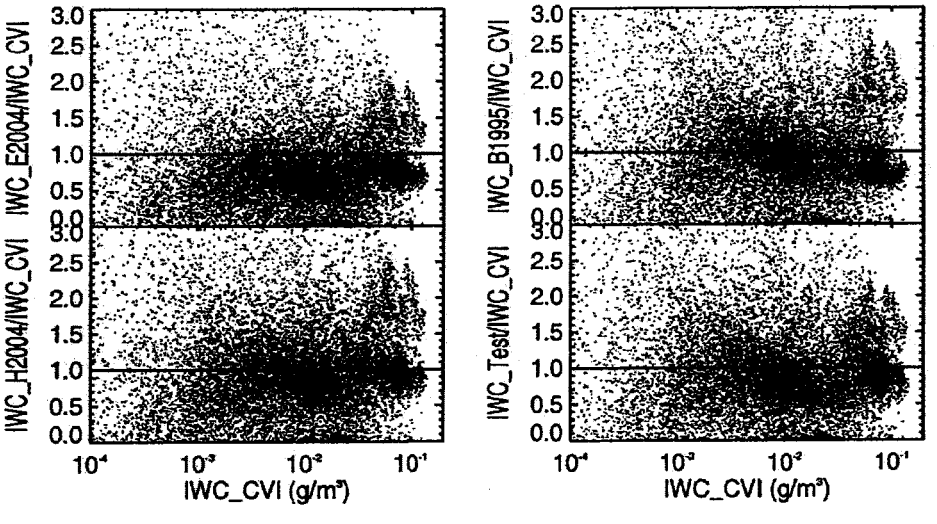

Figure 2. The ratio of calculated IWC with CVI measured as a function of CVI measured IWC. Each panel corresponds to a mass-length relationship given in Fig.1. Note the contribution of missed small ice crystals is assumed to be ~15% of the total IWC on average.

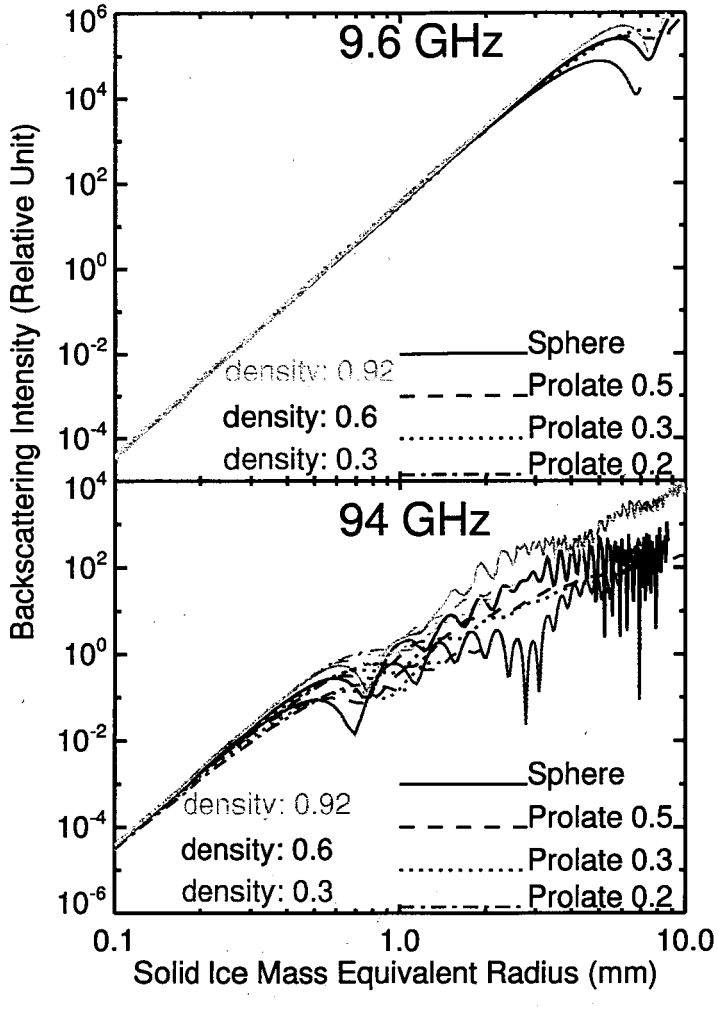

Figure 3. The 9.6 and 94 GHz backscattering intensities of different shape and bulk density ice crystals as a function of the radius of the solid mass equivalent ice sphere. Spheres and prolate spheroids with different aspect ratios are indicated by different line styles, and different bulk densities are shown with different gray shades.

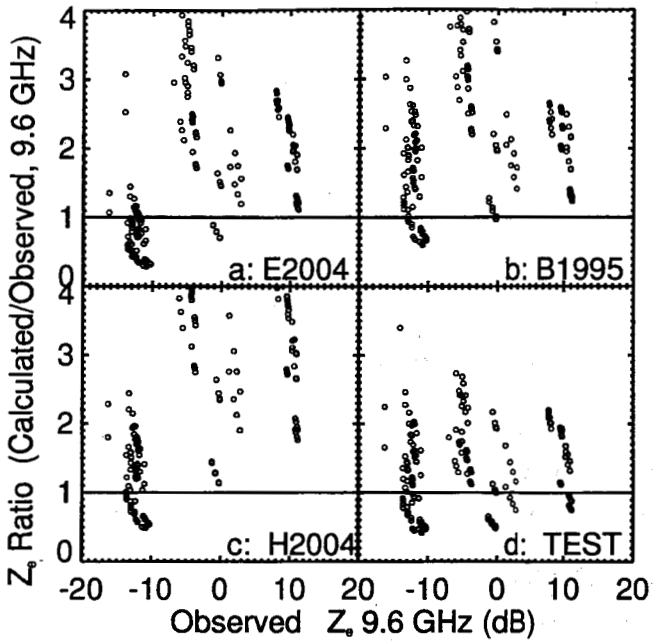

Figure 4. The ratios of calculated and observed 9.6 GHz Z_e as a function of observed 9.6 GHz Z_e for four different mass-length relationships based on coincident observations

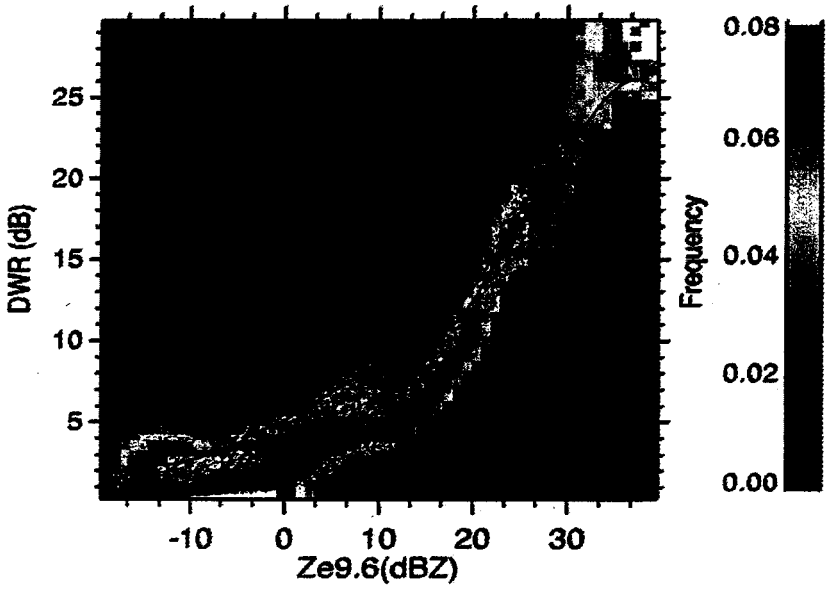

Figure 5. The DWR-Z_e relationship based on CRS and EDOP observations during the CRYSTAL-FACE.

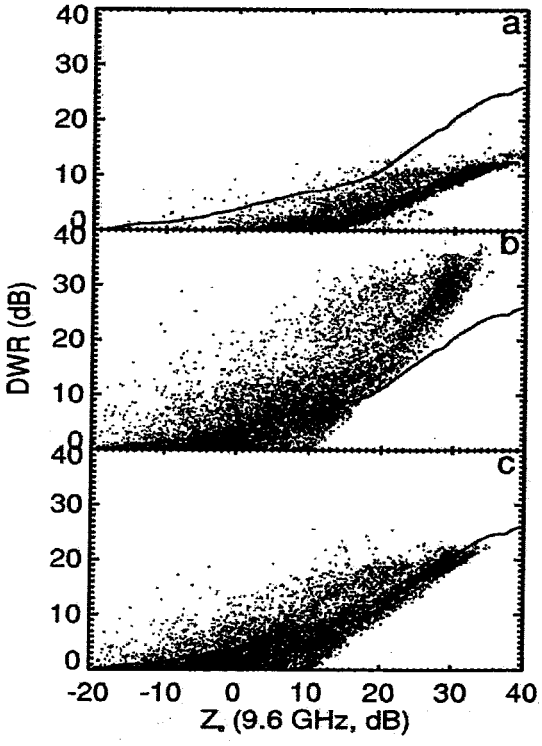

Figure 6. Calculated DWR-Z_e relationships from three different approaches. The solid line represents the mean relationship observed from CRYSTAL-FACE.

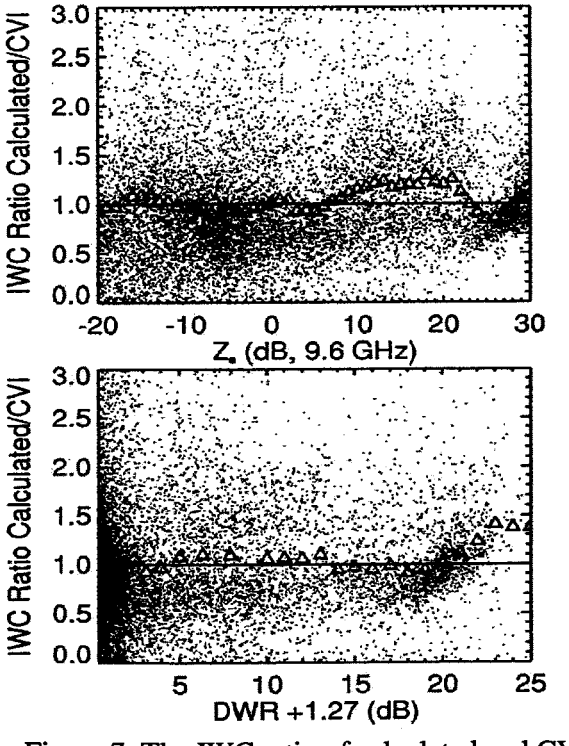

Figure 7. The IWC ratio of calculated and CVI measured as functions of 9.6 GHz Z_e and DWR between 9.6 and 94 GHz. The solid lines indicate the ratio of one, and triangle symbols represent mean ratios within given bin sizes.

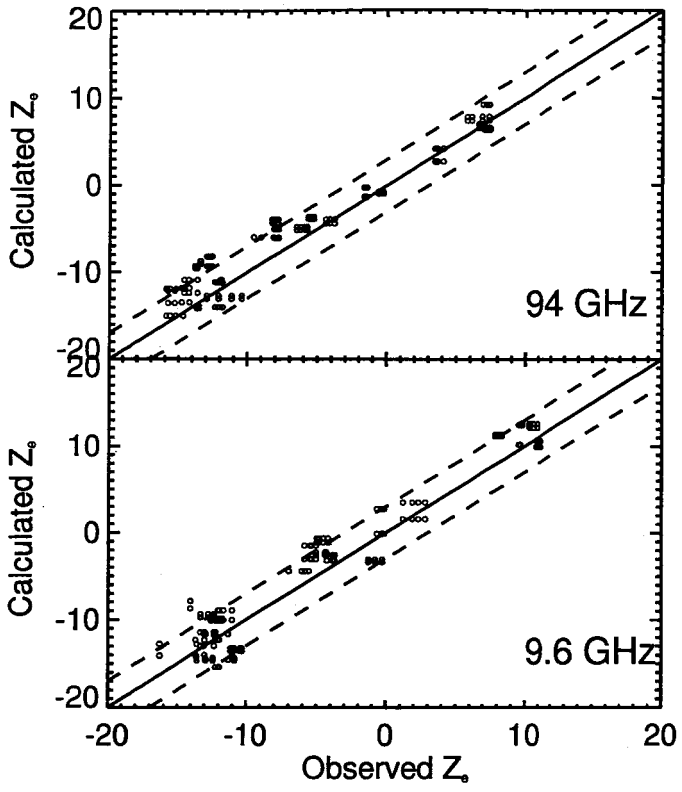

Figure 8. Comparison of calculated Z_e with observed Z_e at 9.6 and 94 GHz for collocated radar and *in situ* observations. The solid line is the 1:1 line and the dashed lines indicate a ± 3dB region about the 1:1 line.

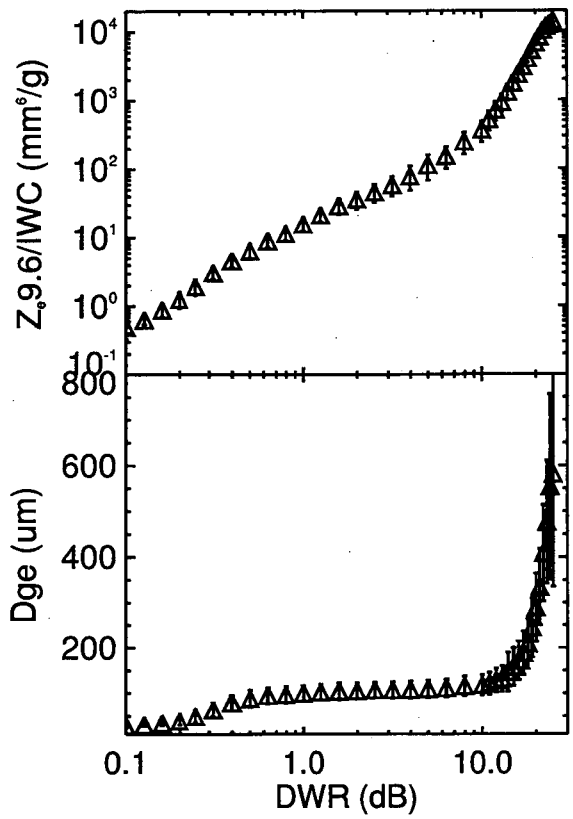

Figure 9. The mean and standard deviation of IWC and D_{ge} as a function of DWR between 9.6 and 94 GHz calculated based on all *in situ* size distribution data from the CRYSTAL-FACE. The vertical bars indicate the standard deviation about the mean.

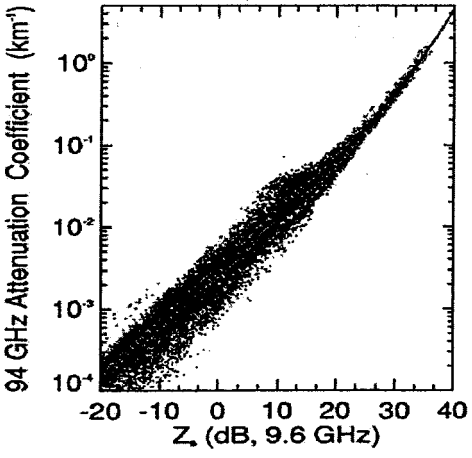

Figure 10. The 94 GHz attenuation coefficient of ice clouds as a function of Z_e at 9.6 GHz. The solid line is a fitted result, and diamond symbols represent means at given Z_e bins. The mean attenuation coefficients for different Z_e bins are represented by diamonds. The solid line is the fitted result of mean values.

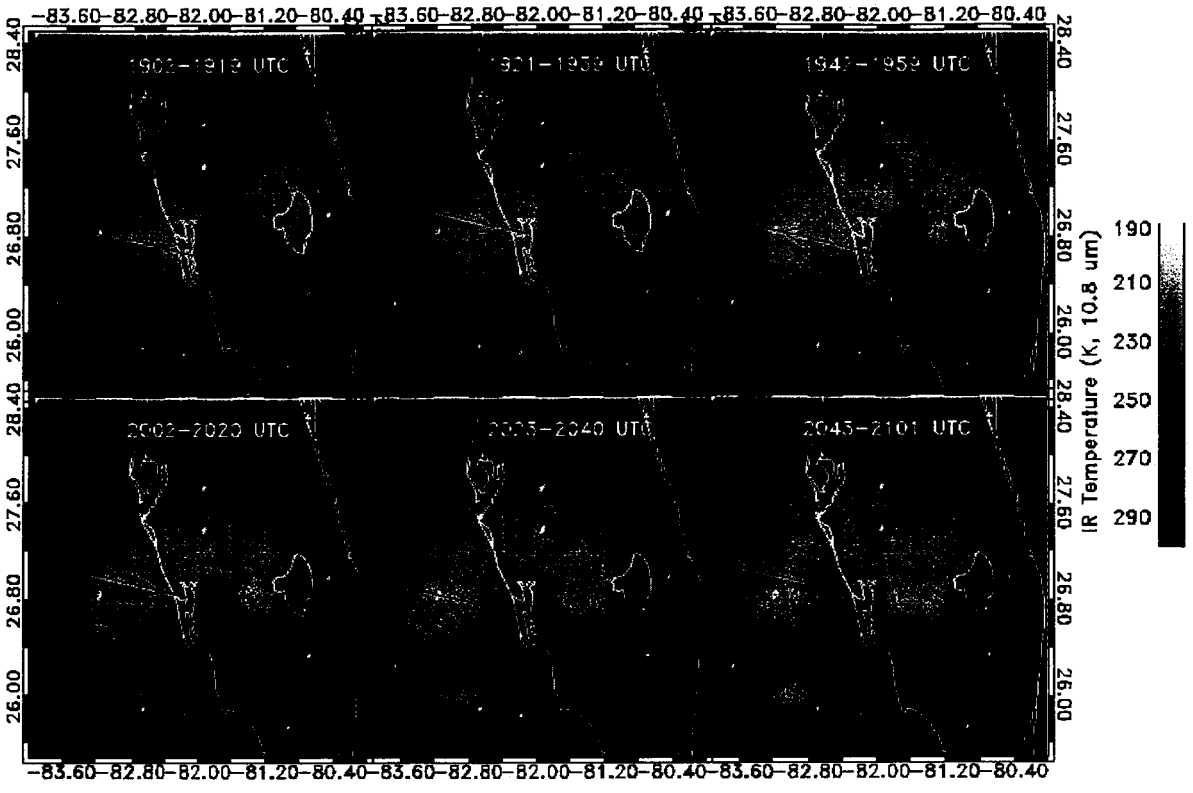

Figure 11. GOES IR images with ER-2 flight tracks (solid black lines) during six periods observed on 29 July 2002 over the west coast of Florida. Arrows in flight tracks indicate the flight direction.

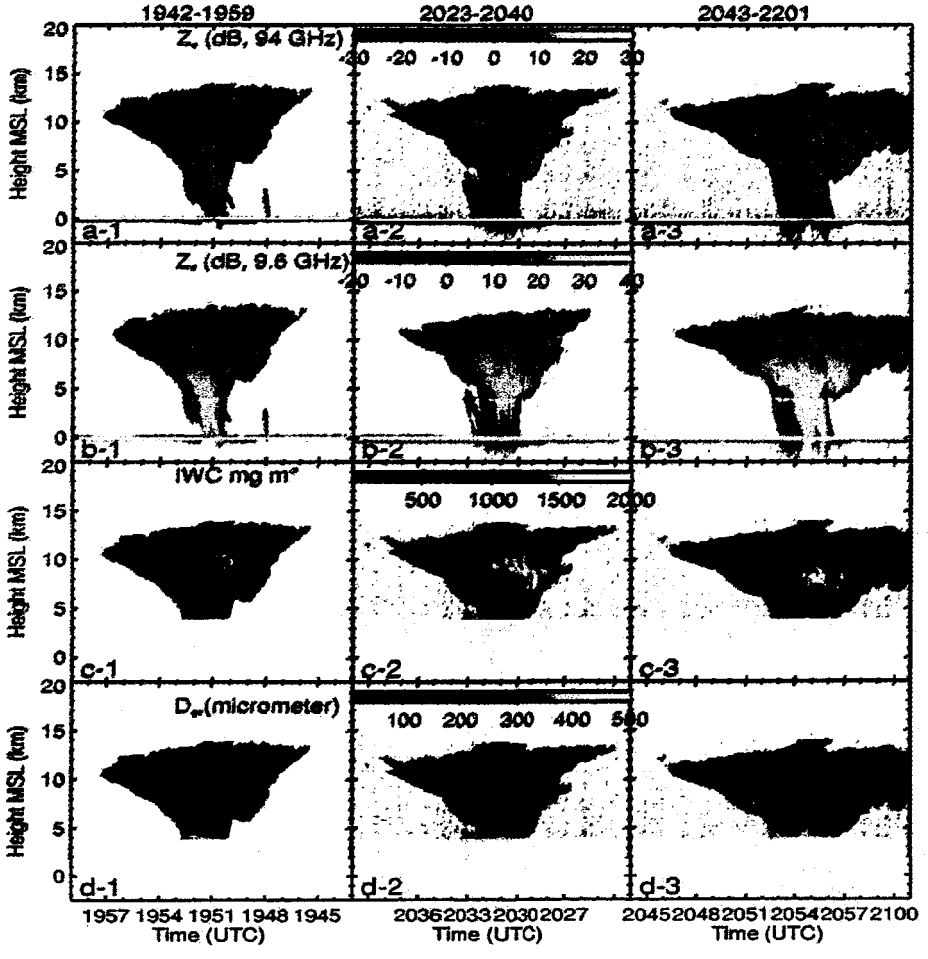

Figure 12. The time-height cross-sections of observed 9.6 and 94 GHz Z_e and retrieved IWC and D_{ge} for three flight tracks given in Fig. 11. Each column represents a flight track with time period given at the top. Note the color scales are different for 94 and 9.6 GHz Z_e. The cross-sections are plotted in the same east-to-west orientation with west on the left side.

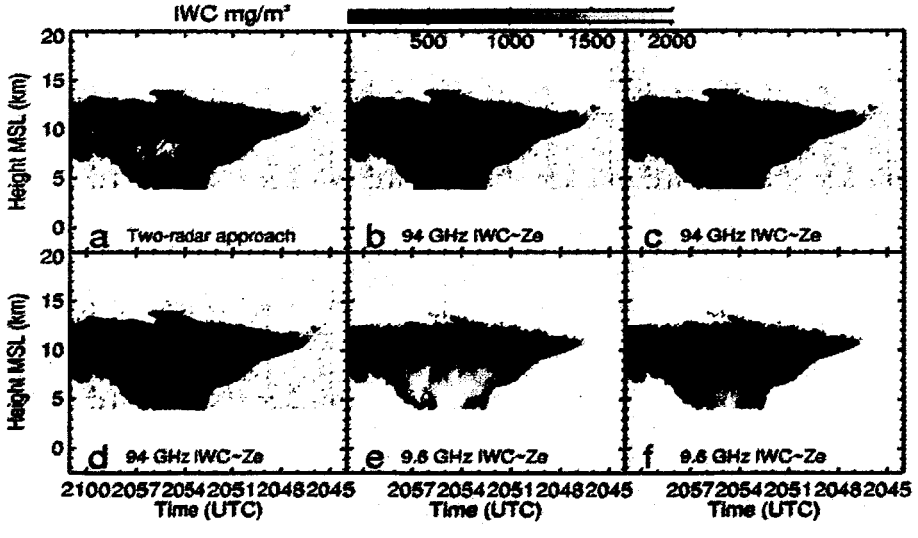

Figure 13: IWC comparison from different approaches: a) two radar approach discussed in this paper, 94 GHz Z-IWC relationships of (b) Liu and Illingworth (2000), (c) Matrosov (2002), and (d) Heymsfield et al. (2005), and 9.6 GHz Z-IWC relationships of (e) $IWC=0.097*Z_e^{0.5}$ and (f) Heymsfield et al. (2005).

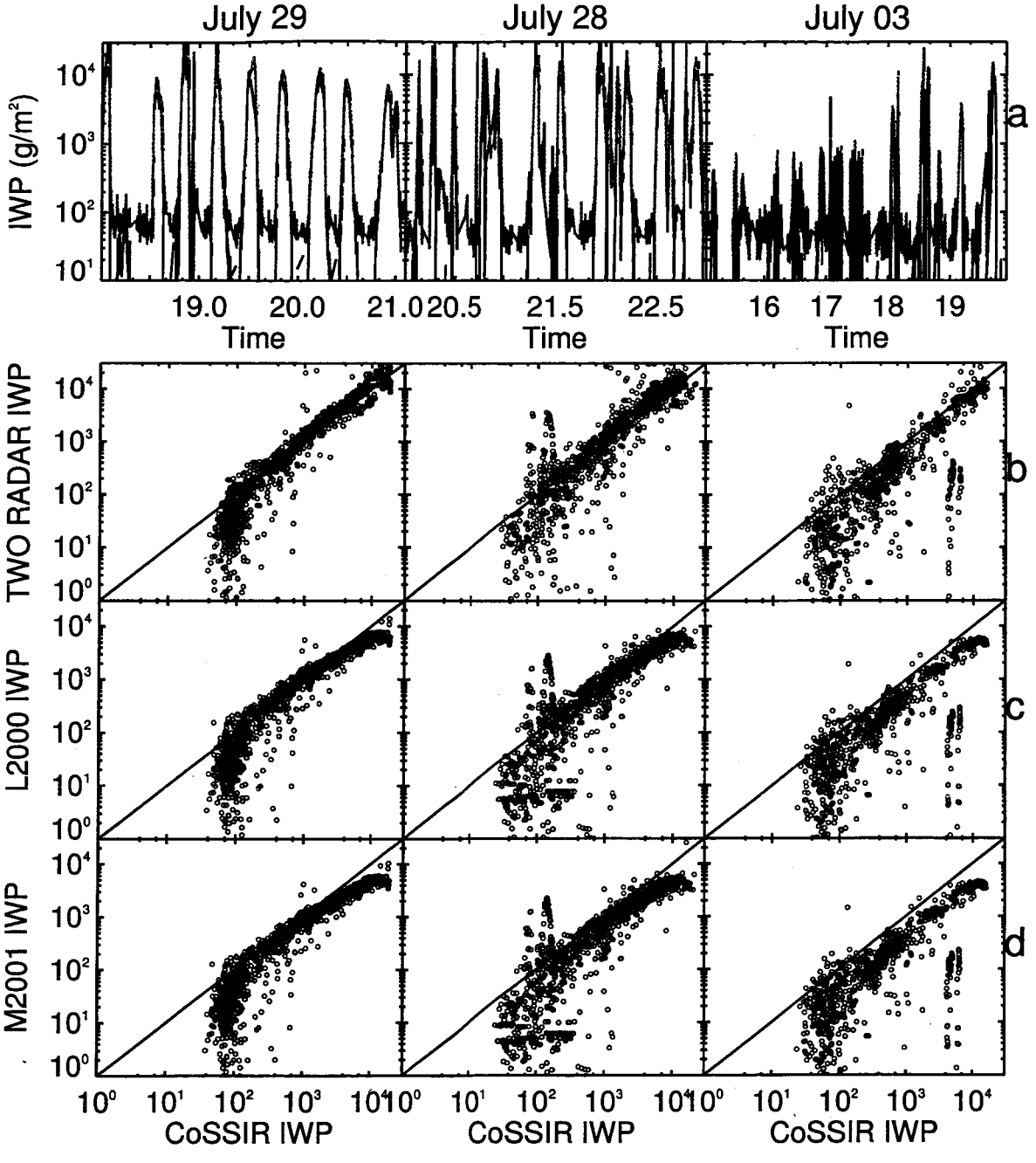

Figure 14: The intercomparison of IWP derived from the two-radar approach, CoSSIR, and two Z_e-IWC relationships based on measurements on 3, 28 and 29 July 2002 during the CRYSTAL-FACE.

Popular Summary

Retrieval of Optically Thick Ice Cloud Microphysical Properties Using Airborne Dual-Wavelength Radar Measurements

By Z. Wang, G.M. Heymsfield, L. Li, and A.J. Heymsfield

Ice clouds play a significant role in the earth's atmospheric water and energy cycles. High cold cirrus clouds affect the Earth's energy balance. We can observe cirrus with many different methods but the global impact of cirrus is still unknown. To improve our weather and climate forecast capability, accurate representations of these ice regions are needed in models. The accuracy of retrievals of ice properties is improving through use of a variety of remote sensors. While there have been substantial advances in our remote sensing capability, it is still difficult to obtain properties of the ice with sufficient accuracy. For clouds that are less transparent, multi-frequency microwave measurements are the most suitable for retrieving properties of the vertical structure of ice properties.

In this study, we will develop an algorithm to profile optically thick ice cloud properties by using airborne 9.6 and 94 GHz radar measurements from the NASA ER-2 high-altitude (~20 km) aircraft during the CRYSTAL-FACE field campaign in 2002. The CRYSTAL-FACE field campaign provided a rich data set to allow us to examine the necessary assumptions used for the algorithm development, so that more realistic assumptions could be used to improve the accuracy of the algorithm. The ER-2 radars take advantage of higher radar sensitivity and higher resolution measurements of upper tropospheric clouds since the cloud top is closer to the radar. The new algorithm presented relies on differences in the reflectivities at both wavelengths due to differences in scattering at the two frequencies. The algorithm is applied to observations, and the retrieved ice properties are compared between several indepentent approaches.